1 SPARC is a new driver of early breast tumor progression via TGF-β -dependent mechanism.

- 3 Marianela Sciacca^{1,2}, María del Pilar Carballo³, Ezequiel Lacunza⁴, Lina Marino³, Paola Noelia
- 4 Cardozo⁵, Naira Rodríguez Padilla¹, Tamara López-López⁶, Martin Abba⁴, Laura Courtois⁷, Ivan
- 5 Bieche⁷, Anne Vincent-Salomon⁸, Érica Rojas Bilbao³, Katrina Podsypanina⁹, Mathieu
- 6 Boissan^{10,11}, Philippe Chavrier¹², Ana María Eiján^{1,2*} Pablo J Sáez^{6*} and Catalina Lodillinsky^{1,2*}.

Affiliations

2

7

8

- 9 ¹ Universidad de Buenos Aires, Facultad de Medicina, Instituto de Oncología Ángel H. Roffo,
- 10 Área de Investigación, Buenos Aires, Argentina.
- ² Consejo Nacional de Investigaciones Científicas y Técnicas (CONICET), Buenos Aires,
- 12 Argentina.
- ³ Universidad de Buenos Aires, Facultad de Medicina, Instituto de Oncología Ángel H. Roffo,
- 14 Área Diagnóstica, departamento de patología, Buenos Aires, Argentina.
- ⁴ Centro de Investigaciones Inmunológicas Básicas y Aplicadas (CINIBA), Facultad de Ciencias
- Médicas, Universidad Nacional de La Plata, La Plata, Argentina.
- ⁵ Universidad de Buenos Aires, Facultad de Medicina, Instituto de Oncología Ángel H. Roffo,
- Area Diagnóstica, departamento de Bioterio y Medicina experimental, Buenos Aires, Argentina.
- 19 ⁶ Cell Communication and Migration Laboratory, Institute of Biochemistry and Molecular Cell
- 20 Biology, and Center for Experimental Medicine, University Medical Center Hamburg-Eppendorf,
- 21 Hamburg, Germany.
- ⁷ Genetics Department, Institut Curie, Paris, France.
- ⁸ Department of Pathology, Institut Curie, Paris, France.
- ⁹ Institut Necker Enfants Malades, INSERM U1151, CNRS UMR-8253, Université Paris Cité,
- Paris, France; Institut Curie, PSL Research University, CNRS, Sorbonne Université, UMR3664,
- 26 Paris, France.
- 27 ¹⁰ Sorbonne Université, INSERM, Centre de Recherche Saint-Antoine, Paris, France.
- 28 ¹¹ APHP, Hôpitaux Universitaires Pitié-Salpêtrière-Charles Foix, Laboratoire de Biochimie
- 29 Endocrinienne et Oncologique, Oncobiologie Cellulaire et Moléculaire, Paris, France
- 30 ¹² Institut Curie, CNRS UMR 144, PSL University, 75005 Paris, France

- * These authors contributed equally to this work
- 32 ** To whom correspondence should be addressed.
- 33 Dr Catalina Lodillinsky
- 34 Instituto de Oncología Ángel H. Roffo
- 35 Av San Martin 5417
- 36 C1417 Ciudad. Autónoma de Buenos Aires, Argentina
- 37 Email: clodillinsky@cbc.uba.ar / Tel: +5411-5287-5364

Abstract

38

39

- 40 Ductal carcinoma in situ (DCIS) is a pre-invasive lesion that is thought to be a precursor of
- 41 invasive ductal carcinoma (IDC). The challenge lies in discriminating between DCIS progressors
- and DCIS non-progressors, often resulting in over- or under-treatment in many cases. Membrane
- 43 type 1 (MT1)-matrix metalloproteinase (MMP) has been previously identified as an essential gene
- involved in DCIS progression. Here, RNA-sequencing analysis of MT1-MMP^{high} subpopulation
- derived from invasive breast tumors in the intraductal xenograft model was compared against a
- dataset of human high-grade DCIS, and Secreted Protein Acidic and Cysteine Rich (SPARC) has
- 47 emerged as a master candidate involved in early breast tumor progression.
- 48 We report that SPARC is up-regulated in DCIS as compared to normal breast epithelial tissues,
- 49 and further increased in IDC relative to synchronous DCIS foci. We found a positive correlation
- 50 between SPARC and MT1-MMP expression in DCIS lesions. At the mechanistic level, depletion
- of SPARC reduced MT1-MMP expression, the degradative capacity of the cells and the activation
- of the TGF- β signalling canonical pathway. Pharmacological inhibition of the TGF- β signalling
- 53 pathway decreased SPARC and MT1-MMP at the mRNA and protein level, and concomitantly
- the cell degradative capacity and 3D cell migration. Strikingly, inhibition of the TGF- β signalling
- 55 pathway limits the invasive transition of breast tumors in a new triple-negative mouse intraductal
- 56 syngeneic xenograft model. Moreover, high SPARC expression was positively correlated with
- both, TGF- β and its receptor, TGFBRI, in a basal type of breast cancer collection supporting our
- 58 findings. This study identifies SPARC as a new driver of early breast tumor progression via a
- 59 TGF-β-dependent mechanism, suggesting TGF-β signaling pathway as a potential target for
- patients with high SPARC expression.

Introduction

61

62

65 66

67

68

69 70

71

72

73

74 75

76

77 78

79

80

81

82

83 84

85 86

87

88

89 90

91

92

93

94

95

96

97

Female breast cancer is the most commonly diagnosed cancer type globally as about 2.3 million women are diagnosed with breast cancer, and more than 0.65 million women die from the disease annually¹. The consequences of this disease highlight the need for new molecular targets to predict recurrence and/or progression and improve existing therapies. Depending on the absence or presence of invasion, breast carcinomas are classified as DCIS, defined as an intraductal neoplastic proliferation of epithelial cells that is separated from the breast stroma by an intact layer of basement membrane and myoepithelial cells², or invasive carcinoma (IDC). Although 90% of DCIS are asymptomatic, diagnosis of DCIS has increased considerably with the implementation of population-scale screening imaging methods, currently accounting for up to 30% of new diagnosed cancers³. DCIS comprises a heterogeneous group of neoplastic lesions that differ in their clinical presentation, histological aspects, as well as genomic, molecular and immune profiles⁴⁻⁶. DCIS is generally found adjacent to IDC in the primary tumor. It is considered a (nonobligate) precursor to IDC, but the features that predict progression to more advanced stages are not well defined. Most women with DCIS choose to have breast-sparing surgery. Radiotherapy is indicated in patients undergoing conservative surgery. Hormonal treatment can reduce risk of ipsilateral breast cancer recurrence in women with hormone receptorpositive DCIS⁷. Yet patients with receptor-negative tumors do not have specific treatment. This context shows the importance of identifying new molecular targets for prediction and treatment. MT1-MMP is overexpressed at the invasive front of invasive breast carcinomas and plays an essential role in the DCIS-to-IDC transition8. In the present study, we used transcriptomic data obtained from MT1-MMPhigh and MT1-MMPlow cell population subsets from intraductal MCF10DCIS.com tumor xenografts that identified SPARC as one of the main genes associated with MT1-MMP expression. Here we report an up-regulation of SPARC in DCIS as compared to normal peritumoral breast tissues and further increase in invasive disease components. SPARC expression in advanced stages is not associated with disease progression, identifying SPARC as a gene associated with the early progression of human breast cancer. SPARC expression correlates with MT1-MMP in patient's samples. In vitro, a reduction in SPARC expression lead to a reduction in MT1-MMP. Furthermore, we found transforming growth factor Beta (TGF-β) highly interconnected with SPARC and pharmacological inhibition of TGF-β receptor type I (TGFBRI) reduces both SPARC and MT1-MMP expression. We also set up a new triple negative murine intraductal syngenic model to investigate how TGFRI signalling pathway influence DCISto-IDC transition. Galunisertib decreased the proportion of invasive tumors. Thus, we propose that blockade of the TGFBRI/SPARC/MT1-MMP axis, may offer therapeutic improvements to patients with in situ tumors.

Materials and Methods

Cell Culture

98

99

100

101

103

105106

107

108

109110

111

112

114

117

118

119120

122

123

124

125

126

127128

130

102 MCF10DCIS.com (MCF10DCIS herein) cell line (CVCL 5552) was purchased from Asterand

(Detroit, MI, USA) and maintained in advanced DMEM/F12 media supplemented with 10% fetal

bovine serum (FBS) and 2 mM glutamine at 37°C in 5% CO₂. Murine breast cancer cell line

LM38-LP (CVCL_B7PY)⁹ was maintained in DMEM-F12 medium (Gibco) supplemented with

2 mM L-glutamine, 80 μg/ml gentamycin and 10% FBS (Internegocios, Argentina) in a

humidified atmosphere with 5% CO₂ at 37°C. Serial passages of confluent monolayers were

performed by detaching cells with trypsin (0.25% trypsin and 0.075% EDTA in Ca²⁺ and

Mg²⁺ free PBS). All experiments were performed with mycoplasma-free cells and the human cell

line, MCF10DCIS has been authenticated using STR profiling.

Cell Isolation, transcriptomic analysis and Target Gene Selection

113 Invasive tumors generated after intraductal injection of MCF10DCIS cells in the mammary gland

of SCID mice⁸ were harvested and mechanically dissociated. FACS based on human CD298 (BD

PharmingenTM, clone LNH-94) and MT1-MMP (Millipore Anti-MMP-14, catalytic domain,

clone LEM-2/15.8) antibodies was performed. Based on MT1-MMP expression levels, two

different cell populations defined as MT1-MMPhigh and MT1-MMPlow were obtained. After RNA

purification, samples were processed according to the protocol of SMARTer stranded total RNA

seq Kit-Pico Input Mammalian, and then sequenced using HISeqTM, of Illumina at the Core

Facility of the Institut Curie, Paris, France.

Briefly, FASTO files generated from sequencing each sample were used to align the sequencing

reads to the human genome, producing BAM files. To perform this alignment, we employed the

SubRead package within the R/Bioconductor environment. Following alignment, we used

Trimmomatic to trim the reads, ensuring data quality and accuracy. The BAM files, after

alignment and trimming, were then processed to create a read counts matrix. This matrix served

as the input for DESeq2, another R/Bioconductor package, which was utilized to identify

differentially expressed genes between the two study groups. The entire analysis was conducted

within the R statistical environment

To identify similarities in gene expression between our experimental model and human high-

grade DCIS samples, we compared the list of genes upregulated in the MT1-MMP^{high} population

of our model with those identified in the human DCIS-C1 and DCIS-C2 subsets. As described by Abba et al. (2015)¹⁰, these two DCIS subgroups were defined based on their tumor-intrinsic subtypes, proliferative and immune scores, and activity of specific signaling pathways. The more aggressive DCIS-C1 subgroup, which is highly proliferative and basal-like or ERBB2(+), exhibited signatures of activated regulatory T cells and immunosuppressive complexes, reflecting a tumor-associated immune suppression, indicative of a tumor-associated immunosuppressive phenotype. This classification provided a valuable framework for comparing the gene expression

Human Tissue samples

131

132

133

134135

136

137138

139

140

158

159

- 141 Formalin-Fixed Paraffin-Embedded (FFPE) human breast tumor tissue were collected from three
- different cohort of patients. PIC-BIM cohort: 116 primary breast tumor samples were collected at
- 143 Institut Curie from 2005 to 2006 prior to any radiation, hormonal or chemotherapy treatment.
- Roffo cohort I: 58 primary breast tumors were collected from 2015 to 2016 and Roffo cohort II:
- 57 samples of primary breast tumors harbouring IDC and lymph node metastasis were collected
- from 2015 to 2020 at Instituto de Oncología A. H. Roffo (SI Table S1).

profiles of our experimental model with those of human DCIS.

- All women provided a signed informed consent for future biomarker research studies. Data were
- analyzed anonymously. This study complies with the Declaration of Helsinki, and was approved
- by each institution's internal review and ethics board (Comité de Pilotage du Groupe Sein, Institut
- 150 Curie). Analysis of the human samples by immunohistochemistry (IHC) was performed after
- approval by review board and ethics committee of Instituto Angel H. Roffo (21/18).
- 152 Tumor breast molecular subtypes were defined as follows according to the guidelines of the
- American Society of Clinical Oncology (ASCO)/College of American Pathologists 11,12. Luminal
- A: estrogen-receptor (ER)≥10%, progesterone-receptor (PR)≥20%, Ki-67 <14%; Luminal B:
- 155 ER≥10%, PR<20%, Ki-67≥14%; HER2+: ER<10%, PR<10%, HER2 2+ amplified or 3+; Triple
- negative breast cancers (TNBC): ER<10%, PR<10%, HER2 0/1+ or 2+ non-amplified.
- 157 Clinical and pathological features of patients are summarized in Table S1.

siRNA treatment, Cell viability assay and cell count assay

- 160 Small interfering RNA (siRNA) transfection was performed using 5 nM siRNA with
- Mission®siRNA Trasfection Reagent (Sigma) according to the manufacturer's instructions. The
- following siRNAs were used: esiRNA cDNA target sequence Human siSPARC: EHU002941,
- Mouse siSPARC: EMU088951; MISSION® siRNA Universal Negative Control #1: sic001

- 164 (Sigma). Subconfluently monolayers of tumoral cells (LM38-LP or MCF10DCIS) were silenced
- using siRNA SPARC (according to company specifications). $3x10^3$ cells/100 µl were cultured in
- 96-well plates and RTq-PCR, IF, gelatin degradation assay and cell viability was analyzed 72 h
- after transfection.

172

- 168 For testing the involvement of the TGF-β pathway on cell viability, LM38-LP cell line was treated
- with TGF-β (2 ng/ml, Peprotech) or SB431542 (20 ng/ml, StemCell) for 48 h. Cell viability was
- determined by the Cristal violet assay (Promega).

Quantitative real time PCR

- 173 Total RNA from murine or human cell lines, were isolated with TRIZol Reagent (Invitrogen) as
- described¹³. Briefly, cDNA was synthesized using RT-PCR SuperScript™ III One-Step
- 175 (Invitrogen) and used as template for qPCR analyzing using TransStart Green qPCR SuperMix
- 176 (TransGen Biotech) and reactions were carried out in the CFX96 Real-Time System, C1000-
- 177 Thermal-Cycler. Specific primers for mouse, SPARC Forward: 5'-
- 178 GCCTGGATCTTCTCTCT-3', Reverse: 5'-GTTTGCAATGATGGTTCTGG-3'; MT1-
- 179 MMP Forward: 5'-GCTTTACTGCCAGCGTTC-3', Reverse: 5'-
- 180 CCCACTTATGGATGAAGCAAT-3' was normalized to GAPDH (glyceraldehyde-3-phosphate
- dehydrogenase) expression Forward: 5'-CAAAATGGTGAAGGTCGGTG-3', Reverse: 5'-
- 182 CAATGAAGGGTCGTTGATG-3'. Human primers: SPARC Forward: 5'-
- 183 GCGGAAAATCCCTGCCAGAA-3'; Reverse: 5'-GGCAGGAAGAGTCGAAGGTC-3'; MT1-
- 184 MMP Forward: 5'-CAACATTGGAGGAGACACCCACT-3', Reverse: 5'-
- 185 CCAGGAAGATGTCATTCCATTCA-3' was normalized to TBP (TATA box-binding protein)
- 186 expression Forward: 5'-TGCACAGGAGCCAAGAGTGAA-3', Reverse: 5'-
- 187 CACATCACAGCTCCCCACCA-3'.
- 188 For RT-qPCR on the samples of the breast cancer cohort, total RNA extraction, cDNA synthesis
- and RT-qPCR reaction have been described elsewhere¹⁴. Quantitative values were obtained from
- 190 the cycle number (Ct value) using QuantStudio 7 Flex real-time PCR system (Applied
- 191 Biosystems, Foster City, CA). Data from each sample were normalized on the basis of its content
- in TBP transcripts. TBP encoding the TATA box-binding protein (a component of the DNA-
- binding protein complex TFIID) was selected as an endogenous control due to the moderate level
- of its transcripts and the absence of known TBP retro-pseudogenes (retro-pseudogenes lead to co-
- amplification of contaminating genomic DNA and thus interfere with RT-PCR transcripts, despite
- the use of primers in separate exons). The relative mRNA expression level of each gene, expressed
- as N-fold differences in target gene expression relative to the TBP gene and termed 'Ntarget',

were determined as Ntarget = $2^{\Delta Ctsample}$, where the ΔCt value of the sample was determined by

subtracting the average Ct value of target gene from the average Ct value of TBP gene. The

Ntarget values of the samples were subsequently normalized such that the median Ntarget value

- of the normal breast samples was 1. Primers for MT1-MMP (upper primer, 5'-
- 202 TTGGAGGAGACACCCACTTTGACT-3'; lower primer, 5'-
- 203 CCAGGAAGATGTCATTCCATTCAG-3'), SPARC (upper primer, 5'-
- 204 TGTGGCAGAGGTGACTGAGGTATC -3'; lower primer, 5'-
- 205 TCGGTTTCCTCTGCACCATCA-3') and TBP (upper primer, 5'-
- TGCACAGGAGCCAAGAGTGAA-3'; lower primer, 5'-CACATCACAGCTCCCCACCA-3'),
- were selected with Oligo 6.0 program (National Biosciences, Plymouth, MN).
- 208 Metastasis-free survival (MFS) was determined as the interval between diagnosis and detection
- of the first metastasis. Survival distributions were estimated by the Kaplan-Meier method, and
- 210 the significance of differences between survival rates was ascertained using a log-rank test.
- 211 GraphPad Prism (GraphPad Software) was used for statistical analysis.

Western blot assay

199

200

212

213

226

227

- Subconfluently monolayers of tumor cells (LM38-LP or MCF10DCIS) were silenced for SPARC
- or were treated with or without SB431542. Then, cells were processed for western blot. Briefly,
- cells were gently washed with PBS and lysed using protein extraction lysis buffer (50 mM Tris-
- 217 HCl (pH 8.0); 100 mM NaCl; 1% Triton, 1 mM/ml aprotinin, 1 mM phenylmethylsulfonyl
- 218 fluoride, 2 mg/ml leupeptin and 10 mM EDTA/EGTA). Protein concentration was determined by
- 219 Bradford method according to the manufacturer's instruction (Merk). Aliquots from the cell
- 220 lysates were separated by electrophoresis and analyzed in 10% sodium dodecyl sulfate-
- polyacrylamide gel (SDS-PAGE) and transferred onto a PVDF membrane. After blotting, the
- membrane was incubated with primary antibody followed by a horseradish peroxidase conjugated
- secondary antibody, for 1 h at room temperature. Blots were developed using the ECL detection
- 224 kit and ImageQuant LAS 500 CCD imager (GE Life sciences). Membranes were stripped and
- incubated overnight with Tubulin used as a loading control.

Immunofluorescence analysis

- 228 LM38-LP or MCF10DCIS cells growing in chamber slides with complete medium were silenced
- 229 for SPARC. Subconfluent monolayers were gently washed with cold PBS and processed for
- immunofluorescence. Briefly, slides were fixed with PFA 4% in PBS for 15 minutes and

permeabilized with Triton X-100 0,3%, with a blocking solution containing 5% FBS in PBS for 1h at room temperature. Fixed cells were incubated overnight with the primary antibody and the following day fixed cells were incubated 2h with secondary antibody. Nuclei were counterstained with DAPI (Santa Cruz Biotechnology) and slides were observed in a Nikon EclipseTM E400 fluorescence microscope and photographed with a CoolpixH 995 digital camera. Mean Fluorescence (AU) was quantified by using Image J software.

Fluorescent Gelatin Degradation Assay

Assays of fluorescent gelatin degradation were performed and quantified as previously described¹⁵. Briefly, clean coverslips are incubated with 1:2000 poly-L-lysine (0.5 μg/ml, Sigma) 20 min at room temperature (RT), washed with PBS and incubated with 0.5% glutaraldehyde 15 min RT. Then washed 3 times with PBS and incubated for 10 min at RT the glass slides by inversion on gelatin-A488 (G13186, Invitrogen) placed on Parafilm previously cleaned with 70% ethanol. The coverslip was washed with PBS and incubated with 5 mg/ml sodium borohydrate (Sigma) during 3 min. The coverslip is washed 3 times with PBS, complete medium is added and incubated with cell suspension. The seeded cells were previously treated with TGF-β (2 ng/ml, Peprotech), SB431542 (20 ng/ml, StemCell) or Galunisertib (1 μg/ml) overnight. After 3h of seeding, cells continued to receive the corresponding treatment. Then, cells were fixed 20 min RT with PFA 4% and stained with phalloidin (A22283, Life technologies) and DAPI (Santa Cruz Biotechnology). Slides were observed in a Nikon EclipseTM E400 fluorescence microscope and photographed with a CoolpixH 995 digital camera. The degradation capacity of the cells was determined using Image J, where levels of proteolysis were quantified as negative fluorescent areas.

Migration assays

To monitor cell migration in 3D complex microenvironments we used collagen gels following an established method^{16–18}. The device was fabricated by curing polydimethylsiloxane (PDMS) on a silicone mold with a positive relief of three compartments previously described¹⁷. The resultant PDMS channel was bonded to a glass bottom Petri dish (Fluorodish) at 65°C for 20 min. Then, rat tail type I collagen (Corning) was diluted to a final concentration of 2 mg/mL with 10% 10X PBS by volume and deionized water, the mixture was prepared and kept at 4°C. The pH was adjusted to pH 8.0 with 1 N sodium hydroxide (NaOH). The cells were added in medium with a final concentration of 0,6x10⁶ cells/ml. The gels polymerized after 20 min of incubation at 37°C. After the administration of the corresponding treatments cellular behavior was monitored using

an inverted microscope (Leica Dmi8) equipped with an APO 10x/0.45 PH1, FL L 20x/0.40 CORR

PH1, and APO 40x/0.95 objectives. Images were recorded with an ORCA-Flash4.0 Digital

camera (Hamamatsu Photonics) using the MetaMorph Version 7.10.3.279 software (Molecular

Device). Images were captured every 3 min for 16 h, employing 10x magnification with PH1

phase contrast and binning set to 2.

265266

267268

271

272

273

274

275

276

277

279

280

283

284285

287

288

289

290291

292

293

294

296

297

For 2D migration experiments, 1.5×10^3 cells were plated on a glass bottom dish and treated for 2

h with TGF-β (2 ng/ml, Peprotech) or SB431542 (20 ng/ml, StemCell) and stained with Hoesch

(Invitrogen). Cells were monitored using the same system described for 3D, using 10x

magnification and for a total duration of 4.5 h. Cell tracking was performed by combining

previously described methods^{17,18}. Briefly, raw movies were processed, and later on tracked by

using TrackMate v7 plugin from Fiji (ImageJ) to obtain the main migration parameters ^{17,18}.

Intraductal tumor growth

278 Ten-week-old female BALB/c mice obtained from our Institute Animal Care Division were

inoculated intraductally in the fourth pair of mammary glands with 5x10³ LM38-LP cells as

previously described^{8,19}. After three weeks mice were randomized into 2 groups: Control and

Galunisertib (n=10 per group). After the detection of any palpable tumor (around the fifth week)

Galunisertib was orally administered once a day at a dose of 60mg/kg for 5 days. Then, mammary

glands were harvested and processed for histological procedures. Mice were handled in

accordance with the international procedure for Care and Use of Laboratory Animals. Protocols

were approved by the Institutional Review Board CICUAL, Institute of Oncology Angel H. Roffo

286 (04/2023).

Histological and immunofluorescence analysis of mouse tissue sections

Whole-mount carmine staining and hematoxylin and eosin (H&E) staining of tissue sections were

carried out as previously described²⁰. After whole mount staining, image acquisition was

performed with a Zeiss Stemi 2000-C Stereo Microscope. Quantification of the tumor area was

performed using Image J software. To retrieve antigens on paraffin-embedded tissue samples,

sections were incubated for 20 min in 10 mM sodium citrate buffer, pH 6.0 at 90°C. Then, after

60 min incubation in 5% FCS, sections were incubated overnight with diluted primary antibodies,

washed and further incubated for 2 h at room temperature with appropriate secondary antibodies.

Conventional Hematoxylin (Biopur) and Eosin (Merk) staining was carried out according to

manufacturer's instructions.

Antibodies

Antibodies for immunofluorescence and IHC (conventional or Immunofluorescence) analysis on tissue sections, the following primary antibodies were used: anti-human MT1-MMP (clone LEM-2/15.8, Millipore MAB3328, 1/100) anti-mouse MT1-MMP (PA5-13183, Invitrogen, 1/500), Ki-67 (clone MIB-1, Dako, 1/100), anti-human SPARC (GTX133747 GeneTex), anti-mouse SPARC (PA-5-80062, Invitrogen, 1/500), anti-SMAD-4 (sc-7966, Santa Cruz, 1/200), anti-ki67 (ab1558, Abcam, 1/500), anti-Progesterone receptor A/B (#8757, Cell Signaling, 1/100), anti-Estrogen receptor alfa (sc-542, Santa Cruz, 1/100), anti-HER2/neu (Clon, 4B5, VENTANA anti-HER2/neu, Roche). For immunofluorescence staining of cells in culture: F-actin was stained with Alexa546-phalloidin (A22283, Life technologies, 1/1000) and nuclei with 4',6-diamidino-2-phenylindole (sc-3598, Santa Cruz, 1 µg/ml). Secondary antibodies Goat anti-rabbit A488 (ab150077, abcam, 1/500) or anti mouse A488 (ab150113, abcam, 1/500) were used. For immunoblotting analysis, we used anti p-SMAD 2/3 (Cell Signalling, D27F4 1/500) anti-SMAD 2/3 (sc-133098, Santa Cruz, 1/100), anti-MT1-MMP (clone MAB3328, Millipore, 1/500), β-tubulin (#2146, Cell Signalling, 1/3000) and detection was performed with anti-rabbit IgG Mouse-HRP (RD#HAF007, R&D Systems, 1/5000) or anti-mouse IgG Rabbit-HRP (RD#HAF008, R&D Systems, 1/5000).

Gene Expression Data Analysis

To examine the association and co-expression of genes in breast cancer tissues, we employed scatter plots with regression lines. Data for this analysis was sourced from the TCGA PanCancer Atlas. For assessing the expression of SPARC and MT1-MMP in breast cancer cell lines, we utilized RNA sequencing data from the GSE48213 dataset, which includes comprehensive transcriptional profiling of a breast cancer cell line panel. Additionally, timeline data documenting the progression from normal breast tissue to invasive breast cancer was generously provided by Rebbeck et al²¹. To define the network connectivity and functional associations between coexpressed genes, we utilized the STRING web tool (https://string-db.org/), which provides a comprehensive analysis of known and predicted protein-protein interactions. In addition, we employed the Gene Ontology (GO) analysis tools integrated within STRING to further investigate the biological processes, molecular functions, and cellular components associated with these genes, allowing for a deeper understanding of their potential roles in the studied context.

Statistical analysis

All experiments were repeated almost two times independently. Data are expressed as the mean \pm SD or \pm SEM. Statistical analyses of H-score, protein and mRNA and protein levels, gelatin degradation assay, cell survival, migration and invasion assays were performed using X^2 test, Student's t-test, one-way or two-way analysis of variance using GraphPad Prism (GraphPad Software, La Jolla, CA, USA) as specified in each figure legend with p<0.05 considered significant. For survival analysis, Kaplan–Meier plots were drawn and statistical differences evaluated using the log-rank test. For correlation analysis in cell lines, Pearson's correlation was used. For boxplots indicating gene expression Wilcoxon rank sum test was used. (R software version 3.0.2, R Foundation for Statistical Computing, Institute for Statistics and Mathematics, Vienna, Austria).

Results

Screening for factors involved in the early progression of breast cancer.

We previously reported that MT1-MMP expression is up-regulated in invasive versus *in situ* breast carcinomas and that high MT1-MP levels are correlated with poor clinical outcome in breast cancer patients⁸. In addition, we found that MT1-MMP expression is required for the DCIS-to-invasive transition of breast tumor xenografts formed upon intraductal injection of MCF10DCIS cells in the mammary gland of immunocompromised SCID mice⁸. With the aim of identifying new genes that may contribute to the DCIS-to-IDC transition, we performed RNAseq analysis on MT1-MMP^{high} and MT1-MMP^{low} MCF10DCIS cell populations obtained from MCF10DCIS intraductal tumor xenografts.

Comparison of the two groups identified 47 differentially expressed genes (p value<0.05,

DR<0.05), of which 46 were up-regulated and one was down-regulated. Computational analysis

of the gene list revealed significant enrichment (p<0.01) in biological processes associated with

cell adhesion (mediated by integrins) and the extracellular matrix (among others, collagens and

laminins). These results are consistent with the canonical role of MT1-MMP in extracellular

matrix remodelling, during cell invasion (Figure 1A and Supp file 1).

Abba and colleagues¹⁰, described two distinct DCIS subgroups (aggressive DCIS-C1 and indolent DCIS-C2) based on tumor-intrinsic subtypes, proliferative, immune scores, and activity of specific signaling pathways. With the objective of finding genes potentially involved in the process of DCIS-to-IDC transition we compared upregulated genes in the two DCIS subgroups—relative to normal breast tissue—with upregulated genes in MCF10DCIS MT1-MMP^{high} cells of the xenograft model. Cross-species comparison identified no overlap with DCIS-C2 signature; however, three genes could be detected both in MT1-MMP^{high} and the high-risk human DCIS-C1

signatures (Figure 1B). These genes, Secreted Protein Acidic and rich in cysteine (SPARC),

Cyclooxygenase-2 (PTGS2), and Calcium-Activated Chloride Channel regulator 2 (CLCA2)

showed similar relative expression changes in xenografted MT1-MMPlow vs. high cells and in

primary DCIS_C1 vs. _C2 subgoups (Figure 1C).

We next examined the correlation between the expression of the three candidate genes and MT1-

MMP using public databases. SPARC showed the best correlation with MT1-MMP in breast

cancer samples (from TCGA, p-value: < 2.2e-16) (Figure 1D). In situ immunohistochemistry

(IHC) on xenograft tumor sections showed that SPARC was overexpressed at the invasive edge

of MCF10DCIS tumors, similar to MT1-MMP expression (Figure 1E). Taken together these

results indicated that SPARC is a candidate gene potentially involved in the regulation of the

invasive switch of breast cancer.

SPARC expression increases during early breast cancer progression

We hypothesized that breast cancer progression is associated with an increase in SPARC expression. We stained breast tissues including normal, DCIS and IDC components from two different cohorts of patients (PIC-BIM n=78, and Roffo n=34) for SPARC. In line with previous reports²², SPARC signal was detected in myoepithelial cells of normal mammary ducts, in tumorassociated fibroblasts and in endothelial cells (data not shown). We focused our analysis on carcinoma cells, in which we observed granular cytoplasmic SPARC staining, and calculated an histo (H)-score value based on the percentage of positive cells multiplied by intensity staining on a 0-3 scale (Figure 2A). Overall, SPARC was undetectable in normal breast epithelial cells, but significantly upregulated in tumor tissue. Moreover, in matched DCIS-IDC samples from both cohorts, SPARC levels were higher in IDC than in synchronous DCIS foci (Figure 2A-C). In addition, the proportion of SPARC-positive IDC tumors was higher in high-grade than in lower-grade breast cancers (Figure 2D). When IDC tumors were stratified into breast molecular subtypes, SPARC expression was higher in TNBC (Figure 2E).

Recently, it was proposed that the progression from in situ lesions to IDC involves dual, early and late epithelial-to-mesenchymal transition (EMT) events²¹. Rebbeck and colleagues conducted a pseudo-time analysis using a fitted principal curve on a principal component analysis (PCA) plot of samples, based on the most significant differentially expressed genes between DCIS and co-occurring IDC²¹. This analysis suggested that DCIS samples exhibit varying relationships to their normal counterparts or invasive counterparts, potentially indicating a continuum of tissue states during disease progression within individual patients. To investigate this further, we examined the evolution of SPARC expression across the pseudo-time sequence, correlating it with tumor progression. We found that, similar to EMT genes, SPARC expression exhibited two peaks, suggesting a dynamic role during the transition from DCIS to IDC (Figure 2F, left panel).

 Consistent with immunohistochemistry (IHC) data, SPARC transcript levels were highest in IDC samples (Figure 2F, right panel). These findings support the idea that SPARC may serve as a potential biomarker for the transition from DCIS to IDC, with its increased expression linked to tumor progression. In order to study the association between SPARC and MT1-MMP, we analyzed MT1-MMP expression in the Roffo cohort. We focused our analysis on carcinoma cells in which MT1-MMP staining was observed at the plasma membrane or as a granular cytosolic pattern. We found a statistically significant fraction of DCIS with high MT1-MMP expression coinciding with high expression of SPARC (Figure 2G-I). Thus, SPARC and MT1-MMP are coordinately expressed in the experimental xenograft model (Figure 1E) as well as in patient samples.

To rule out that SPARC is a general progression factor we examined a third cohort of patients, where samples contain both IDC foci and metastatic axillary lymph node tissue. Importantly, lymph node metastases did not contain SPARC-positive cells, in contrast to the primary tumor (Figure supp 1A-C). In addition, SPARC expression by neoplastic cell in IDC was not associated with Relapse Free Survival (Figure supp 1D). These results suggest that SPARC is specifically involved in early invasive progression. SPARC expression is present in the healthy stroma²². In our cohorts, SPARC expression in the tumor stroma did not show significant differences with respect to the molecular subtypes (data not shown). Furthermore, expression of SPARC and MT1-MMP increased concomitantly in cell lines with basal features (Figure supp 2A), consistent with the idea that co-regulation of these genes may be informative only in the neoplastic compartment. To further deepen our analysis, the prognostic power of SPARC and MT1-MMP co-expression was evaluated by RTqPCR in a retrospective cohort of 458 breast cancer patients in which we previously reported that MT1-MMP up-regulation correlated with shorter metastasis-free survival (MFS) (Figure supp 2B, left panel and Ref 8). However, neither SPARC nor combination of SPARC and MT1-MMP expression impacted metastasis-free survival (Figure supp 2B, middle and right panel). This result confirmed that SPARC expression both at mRNA and protein levels was unlikely to contribute to dissemination of breast cancer. Taken together, our findings argued that SPARC was involved exclusively in early progression of breast cancer, a mechanism enhanced by concomitant MT1-MMP up-regulation in the aggressive TNBC subtype.

MT1-MMP mediates the invasive potential of SPARC

With the aim of strengthening our results in an immunocompetent murine model, the role of SPARC in early breast cancer progression was analyzed by using the mouse mammary cancer cell line LM38-LP⁹, which was inoculated in the ductal system of syngeneic mice (Figure sup 4A). Whole-mount and histology staining revealed *in situ* tumors three weeks post-intraductal

438

439 440

441

442

443

444

445

446

447448

449

450

451

452

453

454

455

456

457

458

459

460

461

462

463

464

465

466

467

468

469

470

471

injection of LM38-LP cells. A continuous layer of elongated α-SMA positive myoepithelial cells segregating in situ tumors from the stroma was observed (Figure supp 3B). During the fifth week, LM38-LP tumors spontaneously progressed to invasive lesions characterized by disrupted stromal collagen organization (Figure supp 3AB). These tumors were negative for ER, PR and HER2/neu (Figure supp 3C). Thus, we concluded that LM38-LP xenograft tumors are an appropriate model to study the molecular events involved in the early transition of triple-negative breast cancer in immunocompetent mice. Both the LM38-LP cell line in vitro and tumors generated after intraductal inoculation were positive for MT1-MMP and SPARC with a perinuclear, granular distribution (Figure supp 4A). Knockdown of SPARC by RNAi did not affect cell proliferation or morphology (Figure supp 4B and C). Interestingly, reduction in SPARC expression led to a reduction in MT1-MMP expression in both human MCF10DCIS and murine LM38-LP cells, which correlated with reduction of gelatin degradation capacity (Figure 4CD and supp 4DE). Collectively, these data suggested that SPARC played a pro-invasive role mediated by MT1-MMP. To profile molecules involved in the early transition process, we used a subset of publicly available breast cancer data from the TCGA database to conducted a gene co-expression analysis of the three previously identified genes, SPARC, PTGS2, and CLCA2 together with MMP14 (encoding MT1-MMP) in five breast cancer sample groups Luminal A (LumA, n=473), Luminal B (LumB, n=205), Her2 (n=86), Normal-like (NL, n=73), and Basal (n=185) tumor subtypes and also in an adjacent normal tissue (NAT, n=103) (Supp file 1). Analysis of co-expressed genes from each gene list (coefficient (R) > 0.5 and a p-value < 0.0001), irrespective of breast cancer molecular subtypes, revealed three common genes: MYLK, EGFR, and ADAMTS9 co-expressed with all the four candidate genes (Figure supp 5A). SPARC and MMP14 exhibited the highest number of partners (Figure supp 5B). Focusing on genes coexpressed with individual candidate genes across all breast cancer groups, we identified 161 genes for SPARC, 51 for MMP14, 10 for PTGS2 (except in Basal), and none for CLCA2 (Supp file 1). Notably, only SPARC and MMP14 shared common partners (Figure supp 5B): COL6A2, AEBP1, COL5A1, MMP2, BMP1, COL1A2, COL6A1, COL1A2, PCOLCE, COL3A1, ST3GAL2, SYDE1, GPR124. Further analysis of these 13 shared genes and the three genes coexpressed in all five breast cancer groups revealed a strong association among 80% of them (Figure 4A). The network analyses delineate two main clusters whose genes were functionally associated with the Gene ontology terms collagen, matrix degradation, and the TGF- β signaling pathway (Figure 4A). We could experimentally confirm the involvement of the TGF- β pathway in the SPARCdependent cell survival, as treatment of LM38-LP cells with TGF-β increased cell viability, while

474

475

476

477

478

479

480

481

482

483

484

485

486

487

488

489

490 491

492

493

494

495

496

497

498

499

500

501

502

503

504505

506

507

treatment with TGFBRI inhibitor, SB431542, abolished the survival response (Figure 4B). Although treatment of LM38-LP cells with TGF-β did not affect SPARC expression (data not shown). Inhibition of TGF-β signaling with SB431542 decreased both SPARC and MT1-MMP expression at the mRNA and protein levels, suggesting that activation of TGFBRI signaling contributes to steady-state SPARC and MT1-MMP expression in both LM38-LP and MCF10DCIS cell lines (Figure 4C-F and supp 5C). To test the involvement of SPARC in canonical activation of the TGF-β pathway, we evaluated the phosphorylation status of SMAD2/3 acting downstream of TGFBRI. In cells knocked down for SPARC, p-SMAD 2/3 levels were reduced (Figure 4G), implying that SPARC is required for optimal activation of the TGF-β signaling pathway. Consistent with the loss of MT1-MMP expression following inhibition of TGFBRI, we observed a decrease in gelatinolysis capacity using two different inhibitors, SB431542 or Galunisertib (Figure 5A-D). To determine the effect of TGF-β pathway modulation on motility, we monitored single cell migration in 3D collagen matrices¹⁷, which mimic interstitial migration. TGF-β accelerated the mean speed of LM38-LP cells as compared to control, while treatment with SB431542 reduced cell motility in both LM38-LP and MCF10DCIS cell lines (Figure 5E and Figure supp 5D). Interestingly, the effect of SB431542 treatment was lost in silencing of SPARC in LM38-LP cells, confirming that TGFBRI-induced cell motility is at least partially dependent on SPARC (Figure 5F).

Galunisertib reduces invasion in a syngeneic intraductal mouse model

To further strengthen the above-described functional association between SPARC and TGF-β pathway in an in vivo setting, we used the intraductal injection of LM38-LP cells in syngeneic mice (Figure supp 3A). We observed increased expression of both SPARC and TGFBRI at the invasive tumor edge (Figure supp 5E), suggesting the involvement of the TGF-β molecular pathway in the early breast cancer progression in association with SPARC. To evaluate TGF-β contribution to the *in situ*-to-invasive transition in LM38-LP intraductal tumors, tumor bearing mice were treated with Galunisertib. Based on whole-mount carmine staining of the injected mammary glands and H&E staining of tissue-sections we observed that treatment with Galunisertib decreased the proportion of invasive tumors as compared with the control untreated group (Figure 6A-C). Additionally, the IDC tumor area was significantly larger in untreated vs. Galunisertib-treated tumor xenografts indicating that the IDC component was relatively reduced (Figure 6D). Moreover, Galunisertib-treated tumors contained fewer proliferating cells, as determined by Ki67 staining, and less nuclear SMAD-4, consistent with an effective blockade of TGFBRI signalling. Furthermore, tumors from Galunisertib-treated mice showed lower SPARC and MT1-MMP intensity as compared to untreated controls (Figure 6E-F). Finally, we next examined the correlation between the expression of SPARC and TGF-β and TGFBRI using public

509

510

511

512

513

514

515

516

517

518

519

520

521522

523

524

525526

527

528

529530

531

532

533

534535

536

537

538

539

540

541

542

databases. High SPARC expression was positively correlated with both TGF-β and TGFBRI expression in a basal-type human breast cancer (Figure 6G). Collectively, these data argue that the induced expression of SPARC and MT1-MMP downstream of the TGFBRI would be necessary for in situ to invasive transition in breast cancer **Discussion** Understanding the molecular mechanisms that trigger the formation of invasive tumors from in situ lesions is of paramount importance to select appropriate treatment strategies for women diagnosed with early breast cancer. In the absence of biomarkers that can predict progression many patients receive unnecessary treatment. Experimental models can be used to address this challenge by studying the cellular mechanisms underlying the DCIS-to-IDC transition. We have previously reported an essential role of extracellular matrix-degradative and basement membranebreaching MT1-MMP in DCIS-to-IDC transition using the human-in-mouse intraductal xenograft system of MCF10DCIS cells in immunodeficient mice^{8,19,23}. Here, using computational analysis of gene signatures obtained from MT1-MMP^{high} and MT1-MMPlow cells from intraductal MCF10DCIS cell tumor xeniografts showed a significant enrichment of gens involved in processes associated with cell adhesion and extracellular matrix remodelling²⁴. Alignment of MT1-MMP^{high} cell and high-grade DCIS-C2 cohort¹⁰ gene expression profiles identified three common genes. Up-regulation of these genes in the context of DCIS-to-IDC progression both in the experimental and clinical settings prompted us to investigate these molecules as possible players in the prelude to invasive transition. Among the three candidates, SPARC, was best correlated with MT1-MMP expression. SPARC has been described pro- or anti-tumor roles in different cancers²⁵, such as in advanced breast cancer patients in which low levels of SPARC protein correlated with worse prognosis as compared to tumors expressing high SPARC levels²⁶. In contrast, in multivariate analysis, high SPARC expression was independently predictive for disease-free-survival in all patients^{27,28}. SPARC effect appeared to depend not only on tumor molecular subtype of, but also on intratumoral cell and matrix composition ^{28,29}. We thus hypothesize that SPARC play protumoral role in early breast cancer due to its involvement in DCIS-to-IDC progression. In this work, based on IHC analysis of FFPE tumor samples from three independent cohorts totaling 230 samples and including different stages of invasion, we found that SPARC was upregulated in pre-invasive neoplastic cells compared to normal epithelium. SPARC expression level was also high in the invasive synchronous component in hormone receptor-negative tumors. In other breast cancer subsets, SPARC expression was not associated with disease progression in advanced stages. Furthermore, SPARC expression was not detected in lymph node metastases.

Although strong SPARC expression in the tumor stroma was associated with shorter time to

544

545

546

547

548

549

550

551

552

553

554555

556

557

558

559

560

561

562

563

564

565566

567

568

569570

571

572

573

574

575

576

recurrence among DCIS patients²², in this study we centered our investigation on neoplastic epithelial cells. Recent gene expression analysis of over 2,000 individually microdissected ductal lesions revealed that the progressive loss of basement membrane integrity, which signifies transition towards invasive carcinoma, involves two distinct epithelial-to-mesenchymal transition (EMT) events. The initial EMT event occurs early in progression, while a second event happens later, coinciding with convergence of expression profiles between ductal carcinoma in situ (DCIS) and invasive ductal carcinoma (IDC)²¹. Overexpression of SPARC can promote cell migration and invasion and correlates with expression of mesenchymal markers in several types of cancer cells^{30,31}. In addition, SPARC has been shown to increase expression or activation of a number of metalloproteinases in a fibroblastic and inflammatory context³² and in some cancer cells^{33,34}. In this study, we refine and reinforce these observations based on public databases, IHC data in our patient cohorts and in experimental MCF10DCIS tumor xenografts. We identify SPARC-MT1-MMP cooperation as an early protumoral factor and demonstrate that MT1-MMP expression and matrix degradation is reduced in human and mouse breast cancer cells with SPARC knockdown. Comparative analysis of differentially expressed genes between our experimental model and human high-grade DCIS, combined with co-expression and functional analysis in invasive breast cancer tumor subtypes, identified a network of genes that likely collaborate to promote tumor progression. We used STRING to examine the connectivity of the identified genes and found that TGF-β is highly interconnected with SPARC. This finding is consistent with reports indicating that SPARC acts extracellularly as a mediator of TGF-β signalling in various contexts, including fibrosis and EMT promotion in lung cancer cells^{35–37}. In this study, we extend these observations to breast cancer, showing that in tumor cells of human or mouse origin, blocking TGFBRI activity reduces SPARC and MT1-MMP expression. As a consequence, the invasive proprieties of tumor cells, such as matrix degradation and motility are decreased. We speculated that DCIS-to-IDC progression is driven by TGF-β-dependent increase in SPARC and MT1-MMP levels. Secreted SPARC may interact with TGFBRI in tumor microenvironment³⁸. In vitro, treatment with SPARC did not increase p-SMAD levels in tumor cells (data not shown), suggesting that TGFBRI activation is maximal in cells in culture. On the other hand, KO SPARC cells down-modulate p-SMAD2/3. One possible scenario is that basal TGF-β activity induces SPARC expression as part of the first wave of EMT, while secreted SPARC amplifies TGFBRI signaling to induce MT1-MMP expression, participating in the second EMT wave and to DCISto-IDC transition. This leads us to hypothesize that basal levels of SPARC, when secreted,

activates signaling molecular pathway trigged by the TGFBRI such as MT1-MMP expression, one of the target genes of this pathway.

LM38-LP, a triple negative mouse cell line of breast cancer, was positive for SPARC and MT1-MMP. In this work we described for the first time that this cellular model is able to develop in situ tumors after intraductal injection in syngeneic mice. These intraductal tumors spontaneously progress into invasive ones, which makes this model an excellent tool for studying molecular factors involved in early breast cancer progression events. During progression, as soon as microinvasive cell foci appear, recruitment of inflammatory cells is observed (data not shown). Tumor-bearing mice treated with Galunisertib reduced the proportion and tumor area of invasive foci. The proinflammatory role of TGF-β is well known during tumor progression³⁹ and although we cannot rule out that Galunisertib is acting by blocking the immune system, the tumor cells treated with the inhibitor present lower SMAD-4 positive cells compared to Controls. Thus, TGFβ signaling pathway is being blocked by the inhibitor in tumor cells. Similar to what we observed in vitro, SPARC and MT1-MMP expression is in consequence also reduced in Galunisertib treated tumours. All together, these findings lead us to propose that a mechanism that involves activated TGF-β pathway, induces sustained expression levels of SPARC and MT1-MMP, which are responsible for triggering pro-invasive mechanisms responsible for early transition in triplenegative breast cancer. Lately, efforts have been made to develop specific tools that allow better understanding of the molecular signatures accompanying mechanisms that lead to the progression of carcinoma in situ⁴⁰. In this work, we identify SPARC as an essential gene included in a molecular pathway involved during the DCIS-to-IDC transition, and we propose that the TGFBRI/SPARC/MT1-MMP axis may offer therapeutic targets to improve management of patients with *in situ* tumors.

Figure legends

577

578

579

580

581

582

583

584

585

586 587

588

589

590

591

592

593

594

595

596

597

598

599

600

601

602

603

604

605

606

607 608

609

610 611

Figure 1. Screening of factors potentially involved in the early progression of breast cancer.

A. Heat-map obtained after transcriptomic analysis of MT1-MMP^{high} versus MT1-MMP^{low} populations. **B.** Venn diagram of the list of differentially expressed genes between the DCIS-C1 and -C2 subgroups¹⁰ with the genes upregulated in the MT1-MMP^{high} cell subpopulation. **C.** Box and whisker plots showing the expression of genes in MT1-MMP^{high} and MT1-MMP^{low} in the MFC10DCIS.com cell population and in DCIS_C2 versus C1 groups. Upper panel PTGS2: p-value = 0.01965; SPARC: p-value = 0.0255; CLCA2: p-value = 0.001893 comparing MT1-MMP^{high} versus MT1-MMP^{low}. Lower panel: PTGS2: p-value = 0.01389; SPARC: p-value = 0.002101; CLCA2: p-value = 0.02451. **D.** Scatter plot displaying the relationship between SPARC and MT1-MMP expression levels in breast cancer tumors classified into the intrinsic

612 subtypes, based on data from the TCGA breast cancer dataset. The plot includes a linear

regression line (green) representing the best-fit model between the two variables, along with a

95% confidence interval for the regression predictions (blue dashed lines). The regression analysis

shows a correlation coefficient (R) of 0.51 and a p-value < 0.001, indicating a significant positive

association between SPARC and MMP14 gene expression in breast cancer tumors. E. IHQ

illustrating SPARC and MT1-MMP expression in in situ and invasive tumors after intraductal

injection of MCF10DCIS. Scale bar: 50 µm.

613

614

617

618

- 619 Figure 2. Overexpression of SPARC during human breast cancer progression. A.
- 620 Representative SPARC IHC staining in breast peritumoral tissues and synchronous in situ and
- 621 invasive components from one breast carcinoma biopsies. Dotted line separates stroma from de
- DCIS. E: Epithelium; T: Tumor; S: Stroma. Scale bar: 25μm. B, C. SPARC levels using the H-
- 623 score method in the adjacent peritumoral tissues, in situ and invasive breast carcinomas in
- PICBIM's cohort (B)***p=0.0002, Friedman test and in Roffo's cohort (C) ***p<0.0001,
- Friedman test **D**. Proportion of cases regarding low (I and II) or high (III) histological grade
- **p=0.002 X² test, two-side. **E**. H-score of SPARC in IDC tumors of Roffo's cohort regarding
- molecular subtype, ***p<0.0001 Kruskal-Wallis test. F. Left panel: Scatter plot illustrating the
- 628 trend of SPARC expression -log2(CPM)-versus position along the timeline, during the
- progression from normal breast tissue to invasive breast cancer. Right panel: Box-plot illustrating
- 630 SPARC expression into the different groups considered²¹ *p<0.05; ***p<0.001; ****p<0.0001.
- ns non-significant Wilcoxon rank sum test G. Proportion of cases with high or low expression
- level of SPARC and MT1-MMP of consecutive slides. *p=0.0235 X² test, two-side. **H, I**.
- 633 Representative IHQ staining in DCIS components for SPARC and MT1-MMP low (H) and high
- 634 (I) expression levels. Scale bar: 50μm.
- **Figure 3. Pro-invasive role of SPARC mediated by MT1-MMP. A.** LM38-LP murine breast
- cell line was transiently silenced for SPARC expression. Values corresponding to means \pm SEM,
- relativized to their CRL. **** p<0.0001, *p<0.05 using one-side t-test. **B.** SPARC and MT1-
- 639 MMP expression in MCF10DCIS after transiently silenced for SPARC. Values corresponding to
- means \pm SEM, n = 2 independent experiments of relative amounts of mRNA normalized against
- 641 GAPDH and relativized to their CRL*** p<0.0001, **p<0.01 t-test. C. Representative images
- of cells in gelatin. Blue: DAPI, Green: Gelatin, Red: Phalloidin. Magnification bar: 50µm D.
- Quantification of fluorescent gelatin degradation by total cells in LM38-LP cells silenced or non-
- silenced for SPARC. Quantification of 1 assay (n=2). *p<0.05 using one-tailed t-test.
- 645 Figure 4. Rol of TGF-β molecular pathway in the SPARC pro-tumoral process. A.
- Association STRING analysis between the four candidate genes and co expressed genes. **B.**

647 LM38-LP cells were treated with TGF-β (2ng/ml) and SB431542 (10 and 20 ng/ml) for 48 h, cell

viability was evaluated by crystal violet assay. *p<0.05, **p<0.01 by two-way ANOVA, Tukey's

multiple comparisons test vs CRL. Values are means \pm SEM, n=3 independent experiments. C,

- **D.** Expression mRNA level of SPARC (C) and MT1-MMP (D) in LM38-LP cells after SB431542
- treatment (20ng/ml). Values corresponding to means \pm SEM, n = 3 independent experiments of
- relative amounts of mRNA normalized against GAPDH and relativized to their CRL, t-test, ***
- p<0.0001. E, F. Protein levels of SPARC (E) and MT1-MMP (F) in LM38-LP cells after
- SB431542 treatment (20 ng/ml). Values corresponding to means \pm SEM, n = 3. t-test, **p<0.001.
- 655 **G.** SMAD 2/3 phosphorylation was determined in LM38-LP cells transiently silenced for SPARC
- by Western Blot. Representative imaging and quantification. **p=0.0033 Unpaired t test, two-
- 657 tailed, ns=non-significant.
- 658 Figure 5. TGFBRI inhibition reduces matrix-degradative potential and motility of breast
- cancer cells. A. Representative images of the gelatin degradation assay of the murine LM38-LP
- 660 cells treated or not with TGF-β (2 ng/ml) and SB431542 (20 ng/ml). Representative images of
- 661 cells in fluorescent gelatin. Blue: DAPI, Green: Gelatin, Red: Phalloidin. Magnification bar:
- 50μm. **B**. Quantification of fluorescent gelatin degradation by total cells in LM38-LP cells, (n=4).
- *p<0,05, **p<0.001 using ANOVA-one way. **C.** Representative images of the gelatin degradation
- assay of the murine LM38-LP cells treated with Galunisertib (1 µg/ml). **D.** Quantification of
- fluorescent gelatin degradation by total cells in LM38-LP treated or not with Galunisertib (n=3).
- *p<0.05, using one tailed t-test. **E.** Single cell tracking assay in 3D collagen microdevise in
- 667 LM38-LP cells treated or not with TGF-β and SB431542. Violin plot of track mean speed, ***
- p<0.0001, Kruskal-Wallis test. F. Single cell tracking assay in 2D in LM38-LP cells KO SPARC
- treated or not with TGF-β and SB431542. Violin plot of track mean speed, ***p<0.0001, Kruskal-
- 670 Wallis test.
- Figure 6. TGFBRI modulation impairs the in situ to invasive transition in the LM38-LP
- **experimental model. A.** Balb/c mice were intra-nipple injected with LM38-LP cells and treated
- or not with Galunisertib (60 mg/Kg). Representative images of the whole-mount carmine-stained
- glands analyzed 4-5 weeks after injection. IS, in situ; INV, invasive (Ctrl: n=15; Galunisertib
- n=18; LN, lymph node. Scale bar, 1 mm. **B.** Representative images of H&E tumors. Scale bar,
- $50\ \mu m.\ \textbf{C.}\ Phenotypic\ analysis\ of\ intraductal\ xenograft\ tumors\ of\ LM38-LP\ cells\ control\ or\ treated$
- 677 with Galunisertib. Analysis was based on whole-mount and H&E staining at 4–5 weeks after
- 678 intraductal injection. Phenotypic analysis of intraductal xenograft tumors of LM38-LP cells
- treated or not with Galunisertib. The analysis was based on whole-mount Fisher's exact test, p=
- 680 0.0391. **D.** Tumor area per gland comparing progression status in Ctrl group and treated with
- 681 Galunisertib. 2 ways ANOVA, Tukey's multiple comparisons test, p= 0.0418. **E-F** Percentage of
- positive cells for Ki-67, SMAD-4, SPARC and MT1-MMP markers by Immunofluorescence

- analyses in tissue sections in tumors treated or not with Galunisertib with the illustrative image.
- **p<0.01; *** p<0.001, Mann Whitney test, (pooled tumor from n=3 glands per group). Scale
- bar: 50 μm. **G.** Scatter plot displaying the relationship between SPARC and TGF-β (left panel)
- and TGFBRI (right panel) expression levels in breast basal cancer tumors, based on data from the
- 687 TCGA breast cancer dataset. The plot includes a linear regression line (green) representing the
- best-fit model between the two variables, along with a 95% confidence interval for the regression
- predictions (blue dashed lines).
- 690 Figure supplementary 1. SPARC expression in advanced stages. A. SPARC levels using the
- H-score method in the adjacent peritumoral tissues, invasive breast carcinomas and in lymph node
- metastasis (LNM) in Roffo's cohort. EPI vs IDC** p=0.0031, IDC vs LNM* p= 0.0450 Kruskal-
- Wallis test. **B.** Proportion of negative or positive tumors for SPARC EPI vs IDC, **p=0.0017,
- 694 IDC vs LNM *p= 0.03, X² test, two-side. C. Representative SPARC IHC staining in lymph node
- metastasis. **D**. Metastasis-free survival (MFS) curves for IDC tumor patients with low and high
- 696 SPARC expression by IHQ.
- 697 Figure supplementary 2. SPARC and MT1-MMP expression in cell line collection A.
- Expression levels of MT1-MMP (left panel) and SPARC (right panel) in a collection of breast
- cancer cell lines from the GSE48213 dataset, categorized by Luminal (blue) and Basal (red)
- subtypes. **B.** Metastasis-free survival (MFS) curves for breast tumor patients with low and high
- 701 MT1-MMP (left panel, p=0.014) SPARC mRNA expression (middle panel, NS) and the
- 702 combination of both markers (NS) mRNA expression as compared with normal breast tissue. The
- 458 breast tumors were divided into two groups with low (<3) and high (>3) for both markers.
- Figure supplementary 3. A new syngenic intraductal model. A. LM38-LP intraductal model
- characterization. Balb/c mice were intra-nipple injected with LM38-LP cells in the foth mammary
- 706 glands. Whole-mount and H&E images of in situ, microinvasive and invasive stage of tumors, at
- 3, 4 and 5 weeks respectively after intraductal inoculation. Scale bar: 50 μm. **B.** Representative
- 708 ER, PR and HER2/neu IHC staining in invasive tumors after intraductal injection of LM38-LP.
- 709 Insets corresponds to positive corresponding control: normal epithelial duct (PR and ER) and
- Positive HER2/neu breast tumor. Scale bar: 100 μ m. C. Immunofluorescence analysis of α -SMA
- 711 (red) and DAPI (blue) in *in situ* (upper panel) or invasive (lower panel). Scale bar: 50 µm.
- 712 Figure supplementary 4. Knockdown of SPARC by RNAi did not affect cell proliferation or
- 713 **morphology. A.** Immunofluorescence staining for MT1-MMP (red) and SPARC (red) expression
- 714 in LM38-LP and MCF10DCIS wild type cells. Scale bar: 10 µm. B. Contrast face images
- 715 illustrating morphology of LM38-LP and MCF10DCIS cells transiently silenced or not for
- 716 SPARC. Scale bar: 50 μm. C. Quantification of viable Trypan blue LM38-LP and MCF10DCIS
- 717 cells transiently silenced or not for SPARC. **D**. Immunofluorescence staining for MT1-MMP (red)

- and SPARC (red) expression in MCF10DCIS cells transiently silenced or not for SPARC. Scale
- bar 10 um. E. Quantification of fluorescent signal for MT1-MMP and SPARC expression in
- 720 MCF10DCIS cells transiently silenced or not for SPARC. *** p<0.0001 and *p<0.05 using two
- 721 tailed t-test.
- 722 Figure supplementary 5. Identification of co-expressed genes. A. Euler diagram representing
- the number of genes co-expressed with each of the 4 genes and the overlap between them. **B**.
- Number of genes co-expressed by SPARC and MT1-MMP in the 6 groups of samples considered.
- 725 C. mRNA levels of SPARC (left panel) and MT1-MMP (right panel) in MCF10DCIS cells after
- SB431542 treatment (20 ng/ml). Values corresponding to means \pm SEM, n = 3. t-test, **p<0.001.
- 727 **D.** Single cell tracking assay in 3D collagen microdevice in MCF10DCIS cells treated or not with
- TGF-β and SB431542. Violin plot of track mean speed, ***p<0.0001, Kruskal-Wallis test. E.
- 729 Immunofluoresce illustrating SPARC and TGBRI expression in invasive tumors after intraductal
- 730 injection of LM38-LP. Scale bar: 10 μm.

Acknowledgements

731

732

742

743

- 733 The authors acknowledge the Breast Cancer Study Group and the Incentive and Cooperative
- 734 Research Program "Breast cancer: Cell Invasion and Motility" of Institut Curie and all the staff
- of the Department of Pathology of the Diagnostic Area of the Angel Roffo Institute, specially Dr
- 736 Fernando Carrizo, Fernanda Rocca and Gisela Lopez for their continued support. We also thank
- 737 the patients from both institutions for the breast tumor samples. Dr Cecilia Perez Piñero and M.
- 738 Sol Rodriguez for IHQ of PR and ER assistance. Authors also thank Dr Rebbeck for generously
- providing the timeline data documenting progression from normal breast tissue to invasive breast
- cancer. We also thank A. V. Failla and the UKE Microscopy Imaging Facility (UMIF) under the
- 741 DFG Research Infrastructure Portal: RI-00489.

Author contribution

- 744 M.S. performed in vitro and vivo experiments, analysed the data and participated in the article
- conceptualization. M.P.C. contributed for the collection of the samples at the Institut, L.M.
- performed IHQ staing. M.P.C., C.L. and L.M. analysed clinical samples. E.L. and M.A performed
- 747 the RNAseq analysis and analysed public transcriptome data set. N.P.C. assisted in vivo
- experiments. N.R.P, T.L.L. and K.P. performed in vitro experiments. AV-S selected and classified
- 749 patients from PICBIM. E.R.B. supervised patient's analysis. L.C and I.B. provided and analyzed
- 750 clinical sample data. M.B., P.C., A.M.E. and P.S. assisted with resources, review and editing.
- 751 C.L. supervised the project, designed experiments and wrote the manuscript.

Funding information

752

753

760

761

- Agencia Nacional de Promocion Científica y Tecnologica (ANPCYT), Grant/Award Numbers:
- 755 PICT 2018-03057, PICT 2016-0207; Fundación Fiorini, Grant/Award 2019; 2021 and UBACYT
- 756 20720190100005 BA; ICGex award by Institut Curie. Research Grant from HFSP (Human
- 757 Frontier Science Program Grant No. RGP0032/2022 to P.J.S.), and the Deutsche
- 758 Forschungsgemeinschaft (DFG, German Research Foundation)- Project-ID 335447717-
- 759 SFB13228 (Project A20 to P.J.S.).

References

- 1. Bray F, Laversanne M, Sung H, Ferlay J, Siegel RL, Soerjomataram I, Jemal A. Global
- cancer statistics 2022: GLOBOCAN estimates of incidence and mortality worldwide for
- 764 36 cancers in 185 countries. *CA Cancer J Clin.* 2024;74(3):229-263.
- 765 doi:10.3322/caac.21834
- 766 2. C.F. C, B. W, R.A. S, C.K.Y. N, J. H, T.A. K, J.S. RF. Progression from ductal
- carcinoma in situ to invasive breast cancer: Revisited. *Mol Oncol.* 2013;7(5):859-869.
- 768 http://ovidsp.ovid.com/ovidweb.cgi?T=JS&PAGE=reference&D=emed11&NEWS=N&
- 769 AN=2013589080
- 770 3. Lehman CD, Gatsonis C, Romanoff J, Khan SA, Carlos R, Solin LJ, Badve S,
- 771 McCaskill-Stevens W, Corsetti RL, Rahbar H, Spell DW, Blankstein KB, Han LK,
- Sabol JL, Bumberry JR, Gareen I, Snyder BS, Wagner LI, Miller KD, Sparano JA,
- 773 Comstock C. Association of Magnetic Resonance Imaging and a 12-Gene Expression
- Assay with Breast Ductal Carcinoma in Situ Treatment. JAMA Oncol. 2019;5(7):1036-
- 775 1042. doi:10.1001/jamaoncol.2018.6269
- 576 4. Shaaban AM, Hilton B, Clements K, Provenzano E, Cheung S, Wallis MG, Sawyer E,
- 777 Thomas JS, Hanby AM, Pinder SE, Thompson AM. Pathological features of 11,337
- 778 patients with primary ductal carcinoma in situ (DCIS) and subsequent events: results
- 779 from the UK Sloane Project. *Br J Cancer*. 2021;124(5):1009-1017. doi:10.1038/s41416-
- 780 020-01152-5
- 781 5. Punglia RS, Jiang W, Lipsitz SR, Hughes ME, Schnitt SJ, Hassett MJ, Nekhlyudov L,
- 782 Achacoso N, Edge S, Javid SH, Niland JC, Theriault RL, Wong YN, Habel LA. Clinical
- 783 risk score to predict likelihood of recurrence after ductal carcinoma in situ treated with
- breast-conserving surgery. Breast Cancer Res Treat. 2018;167(3):751-759.

- 785 doi:10.1007/s10549-017-4553-5
- 786 6. Nagasawa S, Kuze Y, Maeda I, Kojima Y, Motoyoshi A, Onishi T, Iwatani T, Yokoe T,
- Koike J, Chosokabe M, Kubota M, Seino H, Suzuki A, Seki M, Tsuchihara K, Inoue E,
- Tsugawa K, Ohta T, Suzuki Y. Genomic profiling reveals heterogeneous populations of
- ductal carcinoma in situ of the breast. *Commun Biol*. 2021;4(1):1-13.
- 790 doi:10.1038/s42003-021-01959-9
- 791 7. Allison KH, Hammond MEH, Dowsett M, McKernin SE, Carey LA, Fitzgibbons PL,
- Hayes DF, Lakhani SR, Chavez-MacGregor M, Perlmutter J, Perou CM, Regan MM,
- Rimm DL, Symmans WF, Torlakovic EE, Varella L, Viale G, Weisberg TF, McShane
- LM, Wolff AC. Estrogen and progesterone receptor testing in breast cancer: ASCO/CAP
- 795 guideline update. *J Clin Oncol*. 2020;38(12):1346-1366. doi:10.1200/JCO.19.02309
- 796 8. Lodillinsky C, Infante E, Guichard A, Chaligné R, Fuhrmann L, Cyrta J, Irondelle M,
- Lagoutte E, Vacher S, Bonsang-Kitzis H, Glukhova M, Reyal F, Bièche I, Vincent-
- Salomon A, Chavrier P. p63/MT1-MMP axis is required for in situ to invasive transition
- 799 in basal-like breast cancer. *Oncogene*. 2016;35(3):344-357. doi:10.1038/onc.2015.87
- 800 9. Bumaschny V, Urtreger A, Diament M, Krasnapolski M, Fiszman G, Klein S, Joffé EB
- de K. Malignant myoepithelial cells are associated with the differentiated papillary
- structure and metastatic ability of a syngeneic murine mammary adenocarcinoma model.
- 803 Breast Cancer Res. 2004;6(2). doi:10.1186/bcr757
- 804 10. Martin C. Abba1, Ting Gong2, Yue Lu2, Jaeho Lee2, Yi Zhong2, Ezequiel Lacunza1,
- 805 Matias Butti 1, Yoko Takata 2, Sally Gaddis 2, Jianjun Shen 2, Marcos R. Estecio 2, 3,
- Aysegul A. Sahin 3 and CMA. A Molecular Portrait of High-Grade Ductal Carcinoma In
- 807 Situ. Cancer Res. 2015;176(1):100–106.
- 808 11. Prat A, Cheang MCU, Martín M, Parker JS, Carrasco E, Caballero R, Tyldesley S,
- Gelmon K, Bernard PS, Nielsen TO, Perou CM. Prognostic significance of progesterone
- receptor-positive tumor cells within immunohistochemically defined luminal a breast
- 811 cancer. J Clin Oncol. 2013;31(2):203-209. doi:10.1200/JCO.2012.43.4134
- 812 12. Wolff AC, Hammond MEH, Hicks DG, Dowsett M, McShane LM, Allison KH, Allred
- DC, Bartlett JMS, Bilous M, Fitzgibbons P, Hanna W, Jenkins RB, Mangu PB, Paik S,
- Perez EA, Press MF, Spears PA, Vance GH, Viale G, Hayes DF. Recommendations for
- 815 human epidermal growth factor receptor 2 testing in breast. *J Clin Oncol*.
- 816 2013;31(31):3997-4013. doi:10.1200/JCO.2013.50.9984
- 817 13. Langle Y V., Belgorosky D, Prack McCormick B, Sahores A, Góngora A, Baldi A,

- 818 Lanari C, Lamb C, Eiján AM. FGFR3 Down-Regulation is Involved in bacillus
- Calmette-Guérin Induced Bladder Tumor Growth Inhibition. *J Urol*. 2016;195(1):188-
- 820 197. doi:10.1016/j.juro.2015.06.093
- 821 14. Bièche I, Parfait B, Tozlu SL, Lidereau R, Vidaud M. Quantitation of androgen receptor
- gene expression in sporadic breast tumors by real-time RT-PCR: Evidence that MYC is
- an AR-regulated gene. *Carcinogenesis*. 2001;22(9):1521-1526.
- 824 doi:10.1093/carcin/22.9.1521
- 825 15. Sakurai-Yageta M, Recchi C, Le Dez G, Sibarita JB, Daviet L, Camonis J, D'Souza-
- Schorey C, Chavrier P. The interaction of IQGAP1 with the exocyst complex is required
- for tumor cell invasion downstream of Cdc42 and RhoA. J Cell Biol. 2008;181(6):985-
- 998. doi:10.1083/jcb.200709076
- 829 16. Saéz PJ, Vargas P, Shoji KF, Harcha PA, Lennon-Duméni AM, Saéz JC. ATP promotes
- the fast migration of dendritic cells through the activity of pannexin 1 channels and
- 831 P2X7 receptors. *Sci Signal*. 2017;10(506):1-12. doi:10.1126/scisignal.aah7107
- 832 17. Sáez PJ, Barbier L, Attia R, Thiam HR, Piel M, Vargas P. Leukocyte migration and
- deformation in collagen gels and microfabricated constrictions. *Methods Mol Biol*.
- 834 2018;1749:361-373. doi:10.1007/978-1-4939-7701-7_26
- 835 18. Clausen BE, Amon L, Backer RA, Berod L, Bopp T, Brand A, Burgdorf S, Chen L, Da
- M, Distler U, Dress RJ, Dudziak D, Dutertre CA, Eich C, Gabele A, Geiger M, Ginhoux
- F, Giusiano L, Godoy GJ, Hamouda AEI, Hatscher L, Heger L, Heidkamp GF,
- Hernandez LC, Jacobi L, Kaszubowski T, Kong WT, Lehmann CHK, López-López T,
- Mahnke K, Nitsche D, Renkawitz J, Reza RA, Sáez PJ, Schlautmann L, Schmitt MT,
- Seichter A, Sielaff M, Sparwasser T, Stoitzner P, Tchitashvili G, Tenzer S, Tochoedo
- NR, Vurnek D, Zink F, Hieronymus T. Guidelines for mouse and human DC functional
- 842 assays. Eur J Immunol. 2023;53(12):1-96. doi:10.1002/eji.202249925
- 843 19. Behbod F, Kittrell FS, LaMarca H, Edwards D, Kerbawy S, Heestand JC, Young E,
- Mukhopadhyay P, Yeh HW, Allred DC, Hu M, Polyak K, Rosen JM, Medina D. An
- 845 intraductal human-in-mouse transplantation model mimics the subtypes of ductal
- 846 carcinoma in situ. *Breast Cancer Res.* 2009;11(5):1-11. doi:10.1186/bcr2358
- 20. Teulière J, Faraldo MM, Shtutman M, Birchmeier W, Huelsken J, Thiery JP, Glukhova
- MA. β-Catenin-Dependent and -Independent Effects of ΔN-Plakoglobin on Epidermal
- Growth and Differentiation. *Mol Cell Biol*. 2004;24(19):8649-8661.
- 850 doi:10.1128/mcb.24.19.8649-8661.2004

- 851 21. Rebbeck CA, Xian J, Bornelöv S, Geradts J, Hobeika A, Geiger H, Alvarez JF,
- Rozhkova E, Nicholls A, Robine N, Lyerly HK, Hannon GJ. Gene expression signatures
- of individual ductal carcinoma in situ lesions identify processes and biomarkers
- associated with progression towards invasive ductal carcinoma. *Nat Commun*.
- 855 2022;13(1). doi:10.1038/s41467-022-30573-4
- 856 22. Witkiewicz AK, Freydin B, Chervoneva I, Potoczek M, Rizzo W, Rui H, Brody JR,
- Schwartz GF, Lisanti MP. Stromal CD10 and SPARC expression in ductal carcinoma in
- situ (DCIS) patients predicts disease recurrence. *Cancer Biol Ther*. 2010;10(4):391-396.
- 859 doi:10.4161/cbt.10.4.12449
- 23. Lodillinsky C, Fuhrmann L, Irondelle M, Pylypenko O, Li XY, Bonsang-Kitzis H, Reyal
- 861 F, Vacher S, Calmel C, De Wever O, Bièche I, Lacombe ML, Eiján AM, Houdusse A,
- Vincent-Salomon A, Weiss SJ, Chavrier P, Boissan M. Metastasis-suppressor NME1
- controls the invasive switch of breast cancer by regulating MT1-MMP surface clearance.
- *Oncogene*. 2021;40(23):4019-4032. doi:10.1038/s41388-021-01826-1
- 24. Castro-Castro A, Marchesin V, Monteiro P, Lodillinsky C, Rossé C, Chavrier P. Cellular
- and Molecular Mechanisms of MT1-MMP-Dependent Cancer Cell Invasion. *Annu Rev*
- 867 *Cell Dev Biol.* 2016;32:555-576. doi:10.1146/annurev-cellbio-111315-125227
- 868 25. Said N. Role of SPARC in cancer; friend or foe. Ann Carcinog. 2016;1(1):1003.
- 869 26. Nagai MA, Gerhard R, Fregnani JHTG, Nonogaki S, Rierger RB, Netto MM, Soares FA.
- Prognostic value of NDRG1 and SPARC protein expression in breast cancer patients.
- 871 Breast Cancer Res Treat. 2011;126(1):1-14. doi:10.1007/s10549-010-0867-2
- 27. Zhu A, Yuan P, Du F, Hong R, Ding X, Shi X, Fan Y, Wang J, Luo Y, Ma F, Zhang P,
- Li Q, Xu B. SPARC overexpression in primary tumors correlates with disease recurrence
- and overall survival in patients with triple-negative breast cancer. *Oncotarget*.
- 875 2016;7(47):76628-76634. doi:10.18632/oncotarget.10532
- 876 28. Guttlein LN, Benedetti LG, Fresno C, Spallanzani RG, Mansilla SF, Rotondaro C,
- 877 Iraolagoitia XLR, Salvatierra E, Bravo AI, Fernandez EA, Gottifredi V, Zwirner NW,
- Llera AS, Podhajcer OL. Predictive outcomes for HER2-enriched cancer using growth
- and metastasis signatures driven by SPARC. *Mol Cancer Res.* 2017;15(3):304-316.
- 880 doi:10.1158/1541-7786.MCR-16-0243-T
- 881 29. Sangaletti S, Tripodo C, Santangelo A, Castioni N, Portararo P, Gulino A, Botti L,
- Parenza M, Cappetti B, Orlandi R, Tagliabue E, Chiodoni C, Colombo MP.
- Mesenchymal Transition of High-Grade Breast Carcinomas Depends on Extracellular

- Matrix Control of Myeloid Suppressor Cell Activity. *Cell Rep.* 2016;17(1):233-248.
- doi:10.1016/j.celrep.2016.08.075
- 886 30. López-Moncada F, Torres MJ, Lavanderos B, Cerda O, Castellón EA, Contreras HR.
- SPARC Induces E-Cadherin Repression and Enhances Cell Migration through Integrin
- 888 ανβ3 and the Transcription Factor ZEB1 in Prostate Cancer Cells. *Int J Mol Sci*.
- 889 2022;23(11). doi:10.3390/ijms23115874
- 890 31. Hung JY, Yen MC, Jian SF, Wu CY, Chang WA, Liu KT, Hsu YL, Chong IW, Kuo PL.
- Secreted protein acidic and rich in cysteine (SPARC) induces cell migration and
- epithelial mesenchymal transition through WNK1/snail in non-small cell lung cancer.
- 893 *Oncotarget*. 2017;8(38):63691-63702. doi:10.18632/oncotarget.19475
- 32. Tremble PM, Lane TF, Sage EH, Werb Z. SPARC, a secreted protein associated with
- morphogenesis and tissue remodeling, induces expression of metalloproteinases in
- fibroblasts through a novel extracellular matrix-dependent pathway. *J Cell Biol*.
- 897 1993;121(6):1433-1444. doi:10.1083/jcb.121.6.1433
- 898 33. McClung HM, Thomas SL, Osenkowski P, Toth M, Menon P, Raz A, Fridman R,
- Rempel SA. SPARC upregulates MT1-MMP expression, MMP-2 activation, and the
- 900 secretion and cleavage of galectin-3 in U87MG glioma cells. *Neurosci Lett*.
- 901 2007;419(2):172-177. doi:10.1016/j.neulet.2007.04.037
- 902 34. Gilles C, Bassuk JA, Pulyaeva H, Sage EH, Foidart JM, Thompson EW.
- 903 SPARC/osteonectin induces matrix metalloproteinase 2 activation in human breast
- 904 cancer cell lines. *Cancer Res.* 1998;58(23):5529-5536.
- 905 35. M. Onorato A, Fiore E, Bayo J, Casali C, Fernandez-Tomé M, Rodríguez M, Domínguez
- 906 L, Argemi J, Hidalgo F, Favre C, García M, Atorrasagasti C, Mazzolini GD. SPARC
- 907 inhibition accelerates NAFLD-associated hepatocellular carcinoma development by
- dysregulating hepatic lipid metabolism. *Liver Int*. 2021;41(7):1677-1693.
- 909 doi:10.1111/liv.14857
- 910 36. Sun W, Feng J, Yi Q, Xu X, Chen Y, Tang L. SPARC acts as a mediator of TGF-β1 in
- promoting epithelial-to-mesenchymal transition in A549 and H1299 lung cancer cells.
- 912 *BioFactors*. 2018;44(5):453-464. doi:10.1002/biof.1442
- 913 37. Ham SM, Song MJ, Yoon HS, Lee DH, Chung JH, Lee ST. SPARC Is Highly Expressed
- 914 in Young Skin and Promotes Extracellular Matrix Integrity in Fibroblasts via the TGF-β
- 915 Signaling Pathway. *Int J Mol Sci.* 2023;24(15). doi:10.3390/ijms241512179
- 916 38. Francki A, McClure TD, Brekken RA, Motamed K, Murri C, Wang T, Sage EH. SPARC

917 regulates TGF-beta1-dependent signaling in primary glomerular mesangial cells. J Cell Biochem. 2004;91(5):915-925. doi:10.1002/jcb.20008 918 Charles J. David JM. Contextual Determinants of TGF-β Action in Development, 919 39. Immunity and Cancer.; 2018. doi:10.1038/s41580-018-0007-0.Contextual 920 921 40. Risom T, Glass DR, Averbukh I, Liu CC, Baranski A, Kagel A, McCaffrey EF, 922 Greenwald NF, Rivero-Gutiérrez B, Strand SH, Varma S, Kong A, Keren L, Srivastava 923 S, Zhu C, Khair Z, Veis DJ, Deschryver K, Vennam S, Maley C, Hwang ES, Marks JR, 924 Bendall SC, Colditz GA, West RB, Angelo M. Transition to invasive breast cancer is 925 associated with progressive changes in the structure and composition of tumor stroma. 926 Cell. 2022;185(2):299-310.e18. doi:10.1016/j.cell.2021.12.023 927 928

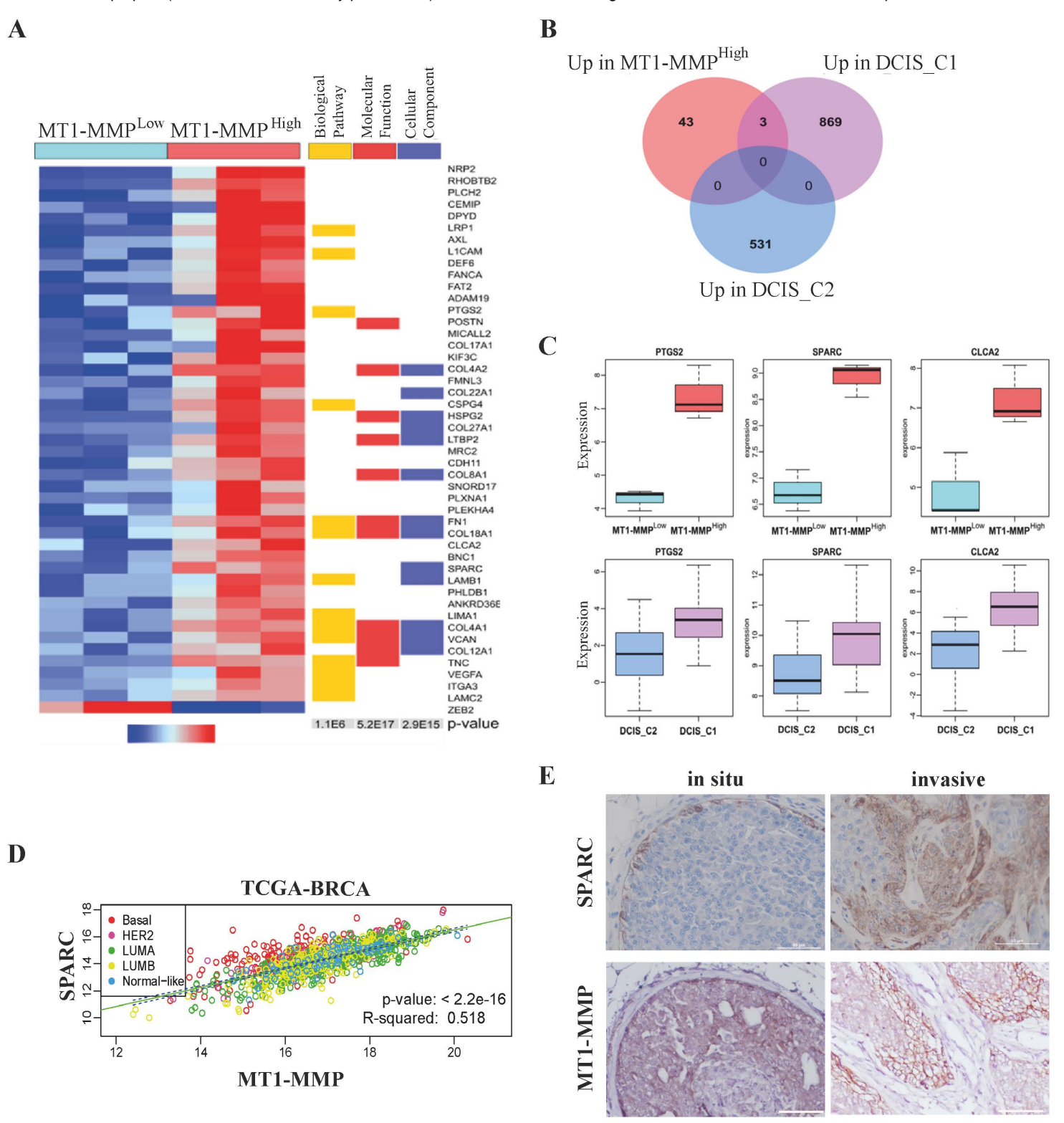


Figure 1

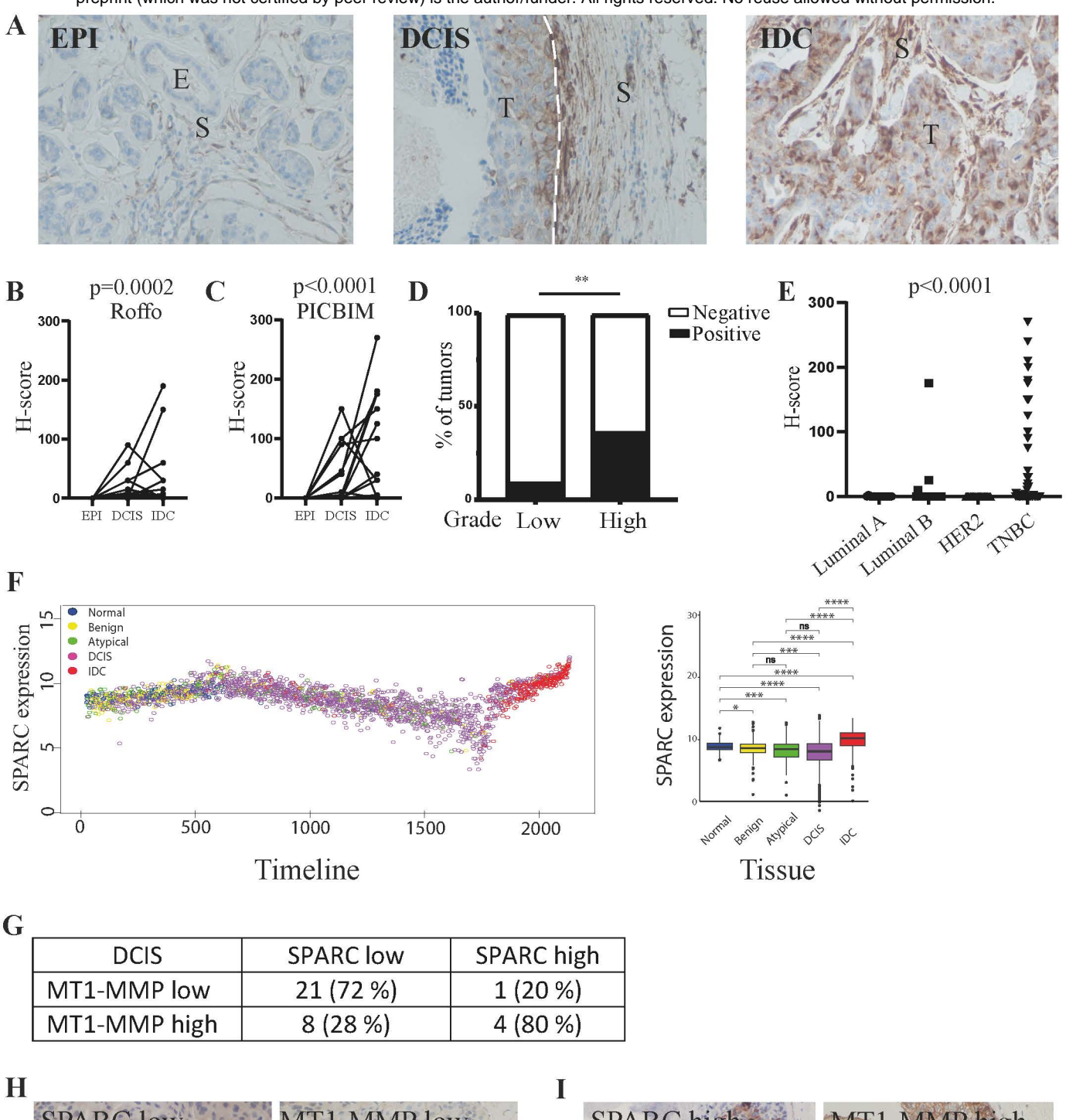




Figure 2

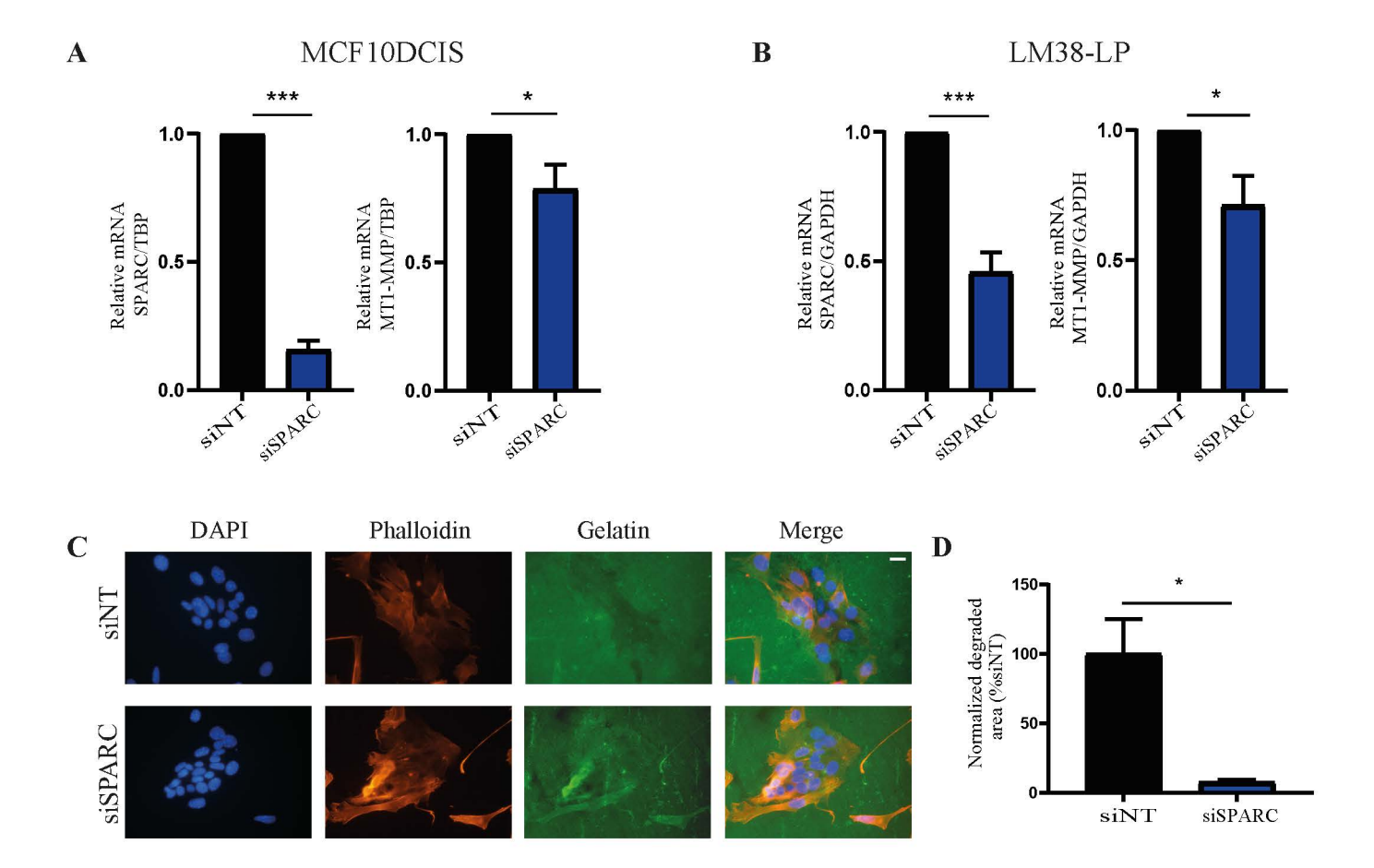


Figure 3

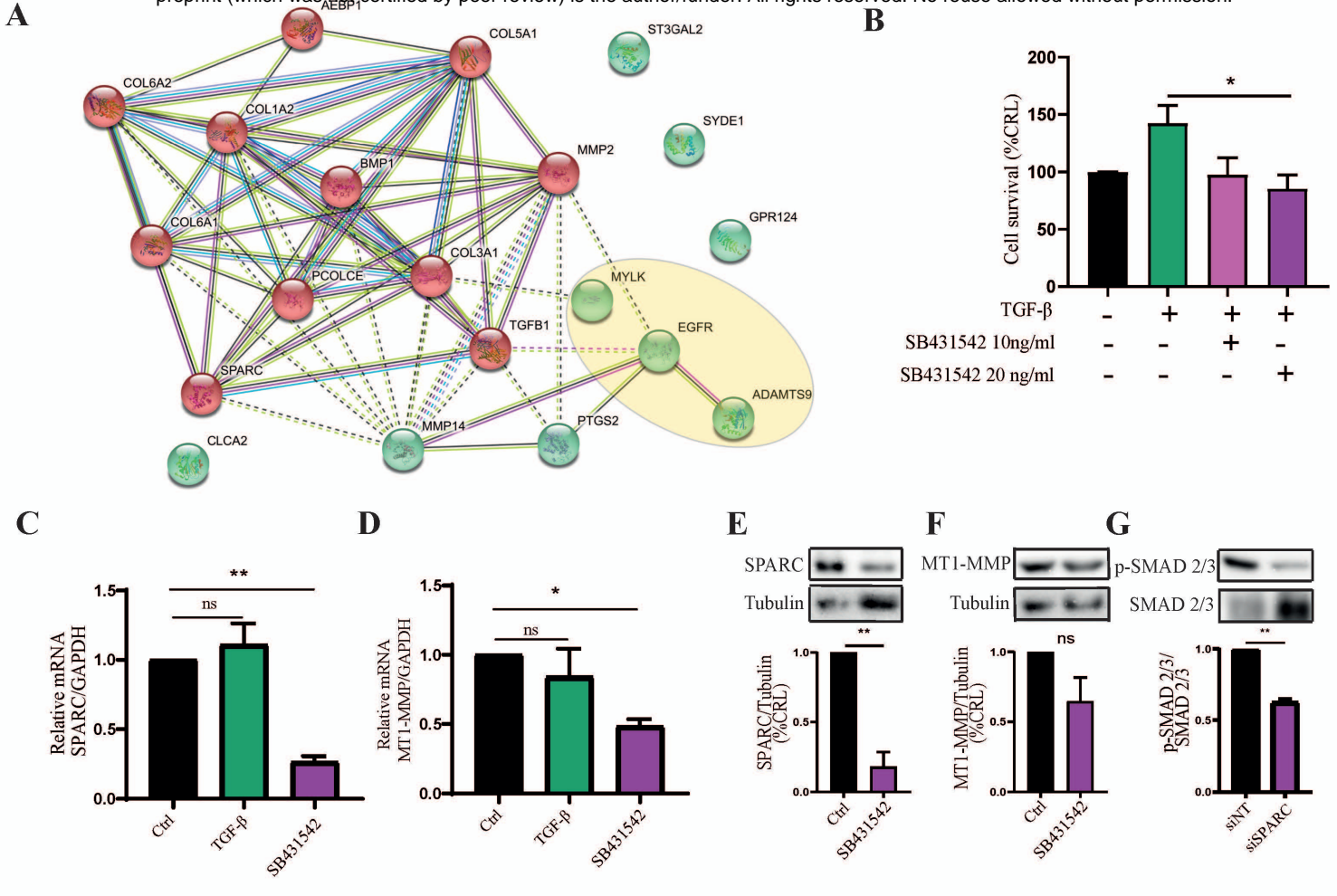


Figure 4

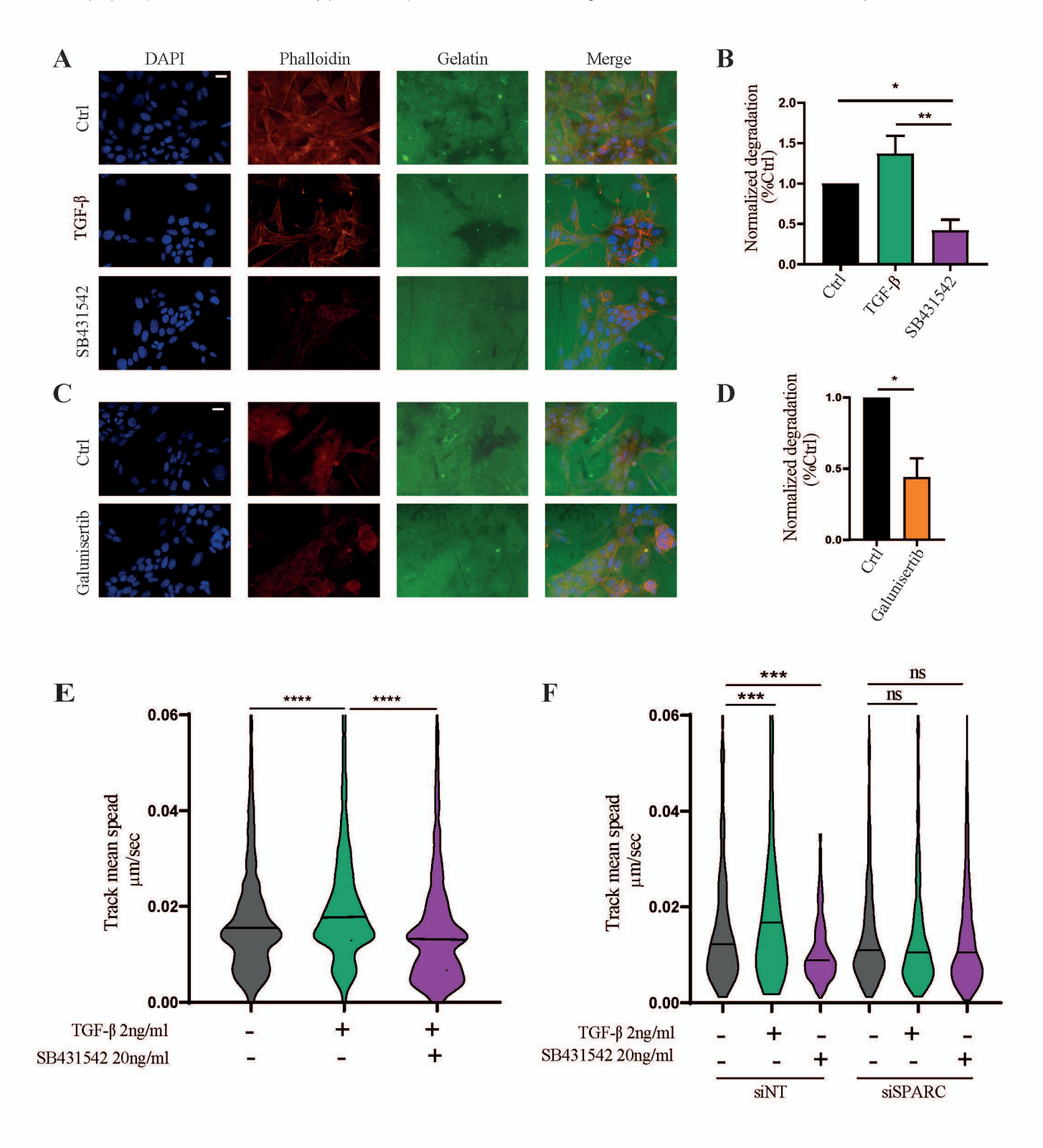


Figure 5

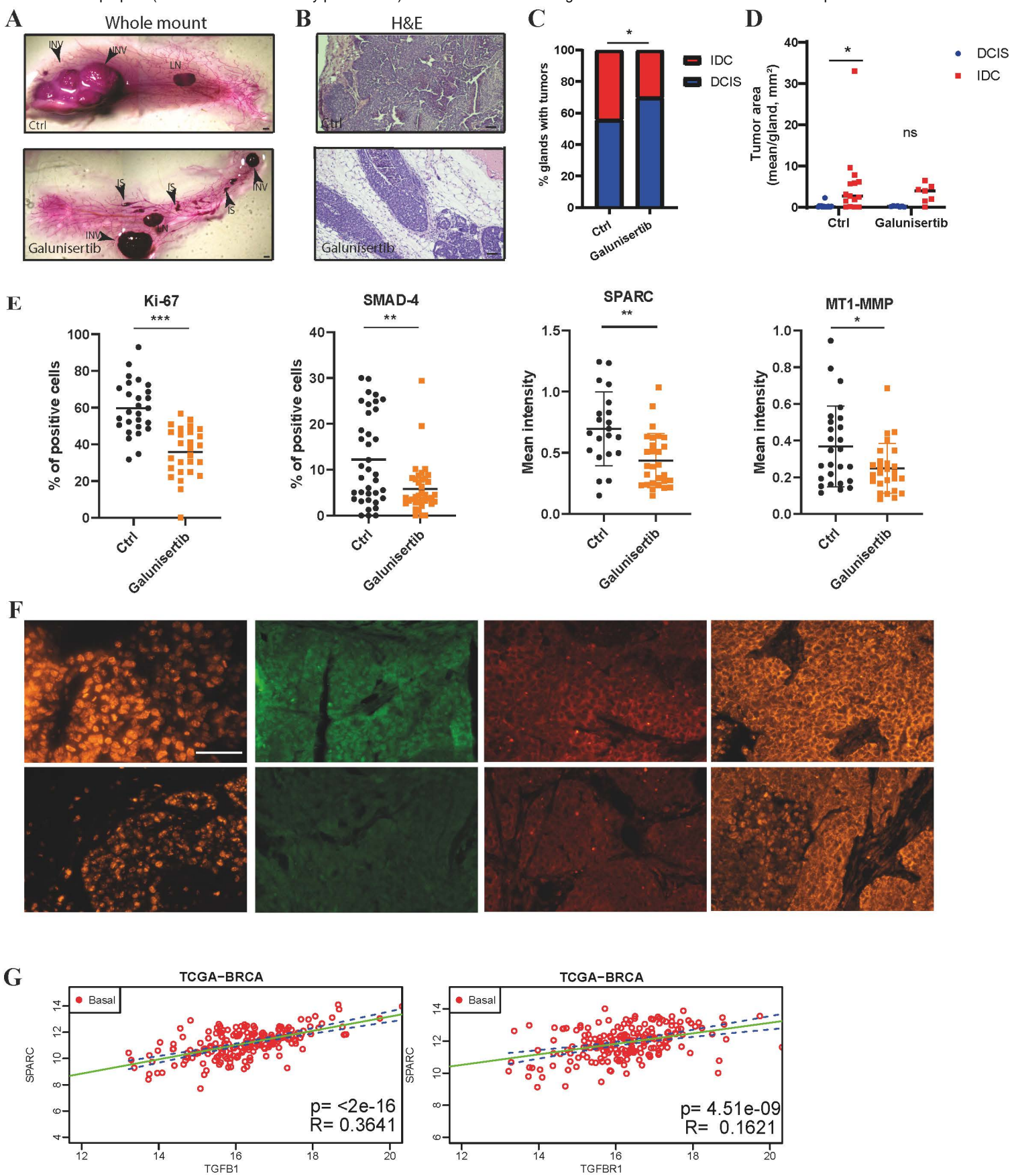


Figure 6